

Anisotropy enhancement of the Casimir-Polder force between a nanoparticle and graphene

S.-A. Biehs*

Institut für Physik, Carl von Ossietzky Universität, D-26111 Oldenburg, Germany

*Corresponding author: *s.age.biehs@uni-oldenburg.de*

G. S. Agarwal

Department of Physics, Oklahoma State University, Stillwater, Oklahoma 74078, USA

(Dated: March 24, 2014)

We derive the analytical expressions for the thermal Casimir-Polder energy and force between a spheroidal nanoparticle above a semi-infinite material and a graphene covered interface. We analyze in detail the Casimir-Polder force between a gold nanoparticle and a single sheet of pristine graphene focusing on the impact of anisotropy. We show that the effect of anisotropy, i.e. the shape and orientation of the spheroidal nanoparticle, has a much larger influence on the force than the tunability of graphene. The effect of tuning and anisotropy both add up such that we observe a force which is between 20-50% of that in the ideal metal case which is much larger than the results found for the Casimir force between a metal halfspace and a layer of graphene.

PACS numbers: 12.20.Ds;42.25.Fx;42.50.Lc;78.67.-n

I. INTRODUCTION

The interaction of atoms and/or nanoparticles with an interface or a cavity is a research topic which has attracted a lot of attention in the past and which is still a vital field of research. Such interactions include for example the change of the radiative life time or Purcell effect¹ close to an interface or in a cavity, the energy transfer between a nanoparticle and a surface^{2,3}, the radiative cooling rate of nanoparticles in close vicinity to a plasmonic system⁴, the Förster resonance energy transfer in the presence of an interface^{5,6}, the Spin-Hall effect close to plasmonic systems⁷ as well as the Casimir-Polder (CP) force⁸.

In particular, the possibility to use materials with special properties as graphene, for instance, has renewed the interest in such studies. So it was shown that graphene allows for controlling the spontaneous emission or local density of states^{9,10} and can enhance the radiative heat transfer between two materials¹¹ and the Förster energy transfer between two atoms in close vicinity of a sheet of graphene^{7,12}. The possibility of changing the electron density of graphene by gating or doping¹³ allows for a certain degree of control of these effects. On the other hand, the Casimir force between two or several sheets of graphene^{14–16}, a sheet of graphene and a metal^{16–19} seems to be extremely small and on the order of some percent of the Casimir force between two perfect metals¹⁷. In addition, the effect of gating or doping has only small influence for gapless graphene^{16,19,20}. Furthermore, it could be shown that by using magnetic fields the Casimir force between two graphene layers can be completely suppressed or even made repulsive due to the quantum Hall effect²¹ an effect which might be useful in the search for Yukawa-like corrections to Newtonian gravity²².

In this work we focus on the CP force between metallic nanoparticles and graphene as sketched in Fig. 1. For a

similar system it was already shown that for large distances the thermal CP force between an atom and suspended graphene has the same value as that between an atom and a perfect metal²³. Furthermore, the possibility to use graphene as a shield for controlling the CP interaction has been investigated²⁴. Here we consider metal nanoparticles instead of atoms and analyze the impact of anisotropy by considering the CP force between oblate and spheroidal nanoparticles and a layer of graphene. We will show that for large distances the CP force converges to the force between a spheroidal nanoparticle and a perfect metal regardless of the shape and orientation of the particle. As observed for the Casimir force the tunability of graphene has little influence on the resulting force and it turns out that the dependence of the CP force on the shape and orientation of the particle can be much larger than the dependence on the Fermi level inside graphene. Finally, we show that the effect of tuning and anisotropy add so that the resulting force attains relatively large values which are between 20-50% of that observed in the ideal metal case.

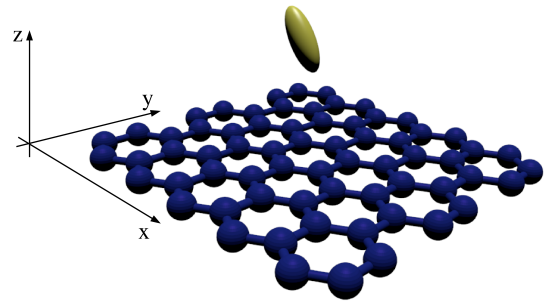


Figure 1. Sketch of a spheroidal gold nanoparticle above a sheet of graphene.

The paper is organized as follows: In Sec. II we de-

rive the general expressions for the CP energy and force between an anisotropic nanoparticle and a halfspace or a graphene-covered halfspace. In Sec. III we introduce the models describing the material properties of gold and graphene which are used in the numerical simulations. Then in Sec. IV and V we discuss numerical results for the CP force between isotropic and spheroidal nanoparticles and a sheet of graphene. Finally, we summarize our results in Sec. VI.

II. CASIMIR-POLDER FORCE

In this section we derive the expression for the CP energy as well as for the CP potential of an in general anisotropic nanoparticle and an interface.

A. Interaction energy

Following the procedure from Ref.¹, the interaction energy between a small particle and a surface induced by fluctuations can be written as

$$H_I = -\frac{1}{2}\langle \mathbf{p}^{\text{ind}} \cdot \mathbf{E}^{\text{fl}} \rangle - \frac{1}{2}\langle \mathbf{p}^{\text{fl}} \cdot \mathbf{E}^{\text{ind}} \rangle, \quad (1)$$

where the induced dipole moment and field in Fourier space are given by

$$\mathbf{p}^{\text{ind}}(\omega) = \epsilon_0 \underline{\underline{\alpha}}(\omega) \cdot \mathbf{E}^{\text{fl}}(\omega), \quad (2)$$

$$\mathbf{E}^{\text{ind}}(\omega) = \omega^2 \mu_0 \mathbf{G}(\omega) \cdot \mathbf{p}^{\text{fl}}(\omega). \quad (3)$$

Then we obtain

$$H_I = -\text{Re} \int_0^\infty \frac{d\omega}{2\pi} \epsilon_0 \alpha_{ij}(\omega) \langle E_j^{\text{fl}}(\omega) E_i^{\text{fl}*}(\omega) \rangle - \text{Re} \int_0^\infty \frac{d\omega}{2\pi} \omega^2 \mu_0 \mathbf{G}_{ij}^*(\omega) \langle p_i^{\text{fl}}(\omega) p_j^{\text{fl}*}(\omega) \rangle \quad (4)$$

taking into account that $\langle p_i^{\text{fl}} p_j^{\text{fl}} \rangle = \langle p_i^{\text{fl}*} p_j^{\text{fl}*} \rangle = 0$ and $\langle E_i^{\text{fl}} E_j^{\text{fl}} \rangle = \langle E_i^{\text{fl}*} E_j^{\text{fl}*} \rangle = 0$. Furthermore, we have already used the fact that the correlation functions are delta correlated with respect to the frequency due to the stationarity of the equilibrium situation. Using the fluctuation-dissipation theorem of second and first kind

$$\langle p_i^{\text{fl}}(\omega) p_j^{\text{fl}*}(\omega) \rangle = \Theta(\omega, T) \frac{2\epsilon_0}{\omega} \text{Im}[\alpha_{ij}(\omega)], \quad (5)$$

$$\langle E_j^{\text{fl}}(\omega) E_i^{\text{fl}*}(\omega) \rangle = \Theta(\omega, T) 2\mu_0 \omega \text{Im}[\mathbf{G}_{ij}(\omega)] \quad (6)$$

where

$$\Theta(\omega, T) = \frac{\hbar\omega}{2} + \frac{\hbar\omega}{e^{\hbar\omega/\beta} - 1} \quad (7)$$

we arrive at

$$H_I = -\text{Im} \int_0^\infty d\omega \frac{\omega}{\pi c^2} \Theta(\omega, T) \mathbf{G}_{ij} \alpha_{ij}. \quad (8)$$

Finally, we perform a Wick rotation ($\omega \rightarrow i\xi$) for zero and nonzero temperatures assuming that the polarizability and the Greens function has no poles nor branchpoints inside the first quadrant. Then we obtain

$$H_I^{T=0} = \int_0^\infty d\xi \frac{\hbar\xi^2}{\pi c^2} \alpha_{ij}(i\xi) \mathbf{G}_{ij}(i\xi), \quad (9)$$

$$H_I^{T \neq 0} = \sum_{n=0}^{\infty}{}' \frac{2k_B T}{c^2} \xi_n^2 \alpha_{ij}(i\xi_n) \mathbf{G}_{ij}(i\xi_n), \quad (10)$$

where the Matsubara frequencies are $\xi_n = 2\pi n \frac{k_B T}{\hbar}$. The prime at the sum sign symbolizes that the term for $n = 0$ has to be multiplied by 1/2. Note, that any magnetic response even that of eddy currents has been neglected²⁵ which can be important for thermal heat transfer^{26,27}.

B. Green's function

Now, we assume that the nanoparticle is in close vicinity to a planar medium at distance d . For determining the CP force only the scattered part of the Green's function is needed, since we are interested in the energy difference $H_I(d) - H_I(d \rightarrow \infty)$. The scattering part of the Green's function close to a planar interface is (for $\mathbf{x} = \mathbf{x}'$ and $z = z' = d$)

$$\mathbf{G}^{(\text{sc})} = \int_0^\infty \frac{d\kappa}{2\pi} \kappa \frac{ie^{i\gamma_0 2d}}{2\gamma_0} [r_s \mathbf{S} + r_p \mathbf{P}] \quad (11)$$

with

$$\mathbf{S} = \begin{pmatrix} \frac{1}{2} & 0 & 0 \\ 0 & \frac{1}{2} & 0 \\ 0 & 0 & 0 \end{pmatrix} \quad (12)$$

and

$$\mathbf{P} = \begin{pmatrix} -\frac{1}{2} \frac{\gamma_0^2}{k_0^2} & 0 & 0 \\ 0 & -\frac{1}{2} \frac{\gamma_0^2}{k_0^2} & 0 \\ 0 & 0 & \frac{1}{2} \frac{\kappa^2}{k_0^2} \end{pmatrix}. \quad (13)$$

Here r_s and r_p are the usual Fresnel reflection coefficients for s- and p-polarized light

$$r_s = \frac{\gamma_0 - \gamma}{\gamma_0 + \gamma} \quad \text{and} \quad r_p = \frac{\gamma_0 \epsilon - \gamma}{\gamma_0 \epsilon + \gamma} \quad (14)$$

introducing the wave vector components along the surface normal inside vacuum (γ_0) and inside a medium (γ) having the permittivity ϵ which are explicitly given by

$$\gamma_0 = \sqrt{\frac{\omega^2}{c^2} - \kappa^2} \quad \text{and} \quad \gamma = \sqrt{\frac{\omega^2}{c^2} \epsilon(\omega) - \kappa^2}. \quad (15)$$

C. Casimir-Polder energy and force

Using the scattered Green's function we obtain for the CP energy performing a Wick rotation ($\omega \rightarrow i\xi$)

$$H_{\text{CP}}^{T=0} = H_I^{T=0}(d) - H_I^{T=0}(d \rightarrow \infty) = \int_0^\infty d\xi \frac{\hbar}{4\pi^2} f(\xi), \quad (16)$$

$$H_{\text{CP}}^{T \neq 0} = H_I^{T \neq 0}(d) - H_I^{T \neq 0}(d \rightarrow \infty) = \sum_{n=0}^\infty \frac{k_B T}{2\pi} f(\xi_n) \quad (17)$$

with

$$f(\xi) = \int_0^\infty d\kappa \kappa \frac{e^{-\tilde{\gamma}_0 2d}}{2\tilde{\gamma}_0} \left[\frac{\xi^2}{c^2} r_s(i\xi) \frac{\alpha_x + \alpha_y}{2} - r_p(i\xi) \left(\frac{\alpha_x + \alpha_y}{2} \tilde{\gamma}_0^2 + \kappa^2 \alpha_z \right) \right] \quad (18)$$

The resulting force is given by

$$F_{\text{CP}}^{T=0} = -\frac{\partial}{\partial d} H_{\text{CP}}^{T=0} = \int_0^\infty d\xi \frac{\hbar}{4\pi^2} \tilde{f}(\xi), \quad (19)$$

$$F_{\text{CP}}^{T \neq 0} = -\frac{\partial}{\partial d} H_{\text{CP}}^{T \neq 0} = \sum_{n=0}^\infty \frac{k_B T}{2\pi} \tilde{f}(\xi_n), \quad (20)$$

where

$$\tilde{f}(\xi) = \int_0^\infty d\kappa \kappa e^{-\tilde{\gamma}_0 2d} \left[\frac{\xi^2}{c^2} r_s(i\xi) \frac{\alpha_x + \alpha_y}{2} - r_p(i\xi) \left(\frac{\alpha_x + \alpha_y}{2} \tilde{\gamma}_0^2 + \kappa^2 \alpha_z \right) \right] \quad (21)$$

with $\tilde{\gamma}_0 = \sqrt{\frac{\xi^2}{c^2} + \kappa^2}$.

D. isotropic nanoparticle

For an isotropic nanoparticle we have

$$\underline{\alpha}(i\xi) = \alpha(i\xi) \mathbb{1}, \quad (22)$$

where $\mathbb{1}$ is the unit matrix. For a spherical nanoparticle the polarizability is determined by the Mie coefficients. For nanoparticles having a radius smaller than the skin depth the polarizability can be approximated by the Clausius-Mosotti like expression

$$\alpha(i\xi) = 4\pi R^3 \frac{\epsilon(i\xi) - 1}{\epsilon(i\xi) + 2}. \quad (23)$$

The function f and \tilde{f} reduce in this case to

$$f(\xi) = \alpha(i\xi) \int_0^\infty d\kappa \kappa \frac{e^{-\tilde{\gamma}_0 2d}}{2\tilde{\gamma}_0} \left[\frac{\xi^2}{c^2} r_s(i\xi) - r_p(i\xi) \left(\frac{\xi^2}{c^2} + 2\kappa^2 \right) \right] \quad (24)$$

and

$$\tilde{f}(\xi) = \alpha(i\xi) \int_0^\infty d\kappa \kappa e^{-\tilde{\gamma}_0 2d} \left[\frac{\xi^2}{c^2} r_s(i\xi) - r_p(i\xi) \left(\frac{\xi^2}{c^2} + 2\kappa^2 \right) \right]. \quad (25)$$

If the medium is an ideal metal, we have $r_s = -1$ and $r_p = 1$ so that

$$f_{\text{IM}}(\xi) = -\alpha(i\xi) \int_0^\infty d\kappa \kappa \frac{e^{-\tilde{\gamma}_0 2d}}{2\tilde{\gamma}_0} \left[2\frac{\xi^2}{c^2} + 2\kappa^2 \right] \quad (26)$$

and

$$\tilde{f}_{\text{IM}}(\xi) = -\alpha(i\xi) \int_0^\infty d\kappa \kappa e^{-\tilde{\gamma}_0 2d} \left[2\frac{\xi^2}{c^2} + 2\kappa^2 \right]. \quad (27)$$

Inserting these functions into the expressions for the CP potential or force gives the corresponding results for a spherical nanoparticle above a perfect metal. In particular, it can be shown that in the retarded and non-retarded regime the CP energy reduces to (see²⁸ for instance)

$$H_{\text{NR}}^{\text{IM}} = -\frac{3\hbar c}{8\pi d^4} \frac{\alpha(0)}{4\pi}, \quad (28)$$

$$H_{\text{R}}^{\text{IM}} = -\frac{k_B T}{4d^3} \frac{\alpha(0)}{4\pi}, \quad (29)$$

so that the CP force is given by

$$F_{\text{NR}}^{\text{IM}} = -\frac{3\hbar c}{2\pi d^5} \frac{\alpha(0)}{4\pi}, \quad (30)$$

$$F_{\text{R}}^{\text{IM}} = -\frac{3k_B T}{4d^4} \frac{\alpha(0)}{4\pi}. \quad (31)$$

Here $\alpha(0)$ is the static expression of the polarizability of the nanoparticle. In order to check the above exact expressions as well as the retarded and nonretarded approximations we have plotted $H^{\text{IM}}/\alpha(0)$ using (26) (see Fig. 2) assuming that $\alpha(i\xi) = \alpha(0)$ for all imaginary frequencies as a function of distance. It can be seen that the non-retarded (retarded) approximation is a very good approximation for distances $d \ll \lambda_{\text{th}}$ ($d \gg \lambda_{\text{th}}$) where $\lambda_{\text{th}} = \hbar c/k_B T$ is about $7.6 \mu\text{m}$ at $T = 300 \text{ K}$. Similar results (not shown here) can be found for F^{IM} .

E. spheroidal nanoparticle

Now, let us assume that we have a spheroidal nanoparticle with radii $R_z \equiv R_a$ and $R_x = R_y \equiv R_b$, i.e. the rotational axis is along the z axis. The nonzero components of the polarizability tensor are then given by the diagonal elements ($i = x, y, z$)

$$\alpha_i(i\xi) = 4\pi R_a R_b^2 \frac{\epsilon(i\xi) - 1}{1 + [\epsilon(i\xi) - 1]L_i} \quad (32)$$

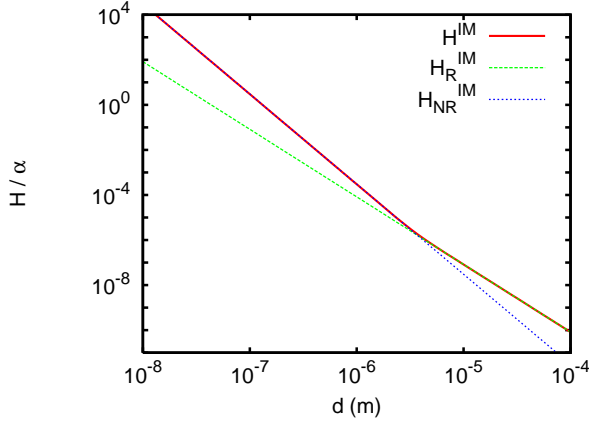


Figure 2. Plot of H^{IM} assuming that $\alpha(i\xi) = \alpha(0)$, $H_{\text{NR}}^{\text{IM}}$ and H_{R}^{IM} normalized to $\alpha(0)$ as a function of distance choosing $T = 300$ K.

where the depolarization factors L_i are for a spheroidal nanoparticle given by the analytical expressions²⁹

$$L_x = L_y = \frac{1}{2}(1 - L_z) \quad (33)$$

$$L_z = \begin{cases} \frac{1-e^2}{e^2} \left[\frac{1}{2e} \ln \left(\frac{1+e}{1-e} \right) - 1 \right], & R_a > R_b \\ \frac{1+e^2}{e^2} \left(1 - \frac{\arctan(e)}{e} \right), & R_a < R_b \end{cases} \quad (34)$$

Note that the expressions for L_z are different for oblate ($R_a < R_b$) and prolate ($R_a > R_b$) nanoparticles as well as the quantity

$$e \equiv \begin{cases} 1 - \frac{R_b^2}{R_a^2}, & R_a > R_b \\ \frac{R_b^2}{R_a^2} - 1, & R_a < R_b \end{cases} \quad (35)$$

Although it would be an easy task to consider all orientations of the spheroidal nanoparticle with respect to a surface, for convenience and clarity we will in the following focus on the CP force between spheroidal nanoparticles above a surface where the rotational axis of the particles are along the surface normal or parallel to the interface.

For the case that the surface is replaced by an ideal metal, the above expressions for f and \tilde{f} which enter in the CP energy and force formulas reduce to

$$f_{\text{IM}}(\xi) = - \int_0^\infty d\kappa \kappa \frac{e^{-\tilde{\gamma}_0 2d}}{2\tilde{\gamma}_0} \left[\left(2\frac{\xi^2}{c^2} + \kappa^2 \right) \frac{\alpha_x + \alpha_y}{2} + \kappa^2 \alpha_z \right], \quad (36)$$

$$\tilde{f}_{\text{IM}}(\xi) = - \int_0^\infty d\kappa \kappa e^{-\tilde{\gamma}_0 2d} \left[\left(2\frac{\xi^2}{c^2} + \kappa^2 \right) \frac{\alpha_x + \alpha_y}{2} + \kappa^2 \alpha_z \right]. \quad (37)$$

Note that depending on the orientation of the rotational axis of the spheroidal nanoparticle with respect to the the interface these expressions can be further simplified.

III. MATERIAL PROPERTIES

In the following we use the above derived expressions to evaluate the CP force between a spherical nanoparticle made of gold and a sheet of graphene. We will compare our results to the CP force for the case that the sheet of graphene is replaced by a gold halfspace. Before presenting the numerical results we introduce the models describing the material properties of the particle and the interface.

A. Gold

For gold we use for convenience the Drude model given by³⁰

$$\epsilon_{\text{Au}}(i\xi) = 1 + \frac{\omega_p^2}{\xi(\xi + \gamma)} \quad (38)$$

with $\omega_p = 1.4 \cdot 10^{16}$ rad/s and $\gamma = 3 \cdot 10^{13}$ rad/s.

When considering a halfspace of Au the reflection coefficients are for $\omega = i\xi$ given by

$$r_s = \frac{\tilde{\gamma}_0 - \tilde{\gamma}}{\tilde{\gamma}_0 + \tilde{\gamma}} \quad \text{and} \quad r_p = \frac{\tilde{\gamma}_0 \epsilon(i\xi) - \tilde{\gamma}}{\tilde{\gamma}_0 \epsilon(i\xi) + \tilde{\gamma}}, \quad (39)$$

where

$$\tilde{\gamma}_0 = \sqrt{\frac{\xi^2}{c^2} + \kappa^2} \quad \text{and} \quad \tilde{\gamma} = \sqrt{\frac{\xi^2}{c^2} \epsilon(i\xi) + \kappa^2}. \quad (40)$$

B. Graphene

The material properties of pristine graphene in the local limit (for the considered distance regime nonlocal effects can be safely neglected) for real frequencies are for the Drude-like term σ_D and the interband contribution σ_I ^{31,32}

$$\sigma_D = \frac{i}{\omega + i/\tau} \frac{2e^2 k_B T}{\pi \hbar^2} \log \left[2 \cosh \left(\frac{E_F}{2k_B T} \right) \right], \quad (41)$$

$$\sigma_I = \frac{e^2 \omega}{i\pi \hbar} \left[- \int_0^\infty d\varepsilon \frac{f_0(-\varepsilon) - f_0(\varepsilon)}{(\omega + i\delta)^2 - 4\varepsilon^2} \right], \quad (42)$$

where

$$f_0 = \frac{1}{e^{(\hbar\varepsilon - \mu)/\beta} + 1}. \quad (43)$$

The relation between the 2D dielectric function and the conductivity for suspended graphene can be written as $\epsilon_{2D} = 1 + i\sigma(\omega)\kappa/2\omega\epsilon_0$ ³³. Hence, by replacing ω by $i\xi$ we obtain

$$\sigma_D = \frac{1}{\xi + i/\tau} \frac{2e^2 k_B T}{\pi \hbar^2} \log \left[2 \cosh \left(\frac{E_F}{2k_B T} \right) \right], \quad (44)$$

$$\sigma_I = \frac{e^2 \xi}{\pi \hbar} \int_0^\infty d\varepsilon \frac{f_0(-\varepsilon) - f_0(\varepsilon)}{\xi^2 + 4\varepsilon^2}. \quad (45)$$

The resulting values of $\sigma = \sigma_I + \sigma_D$ for $E_F = 0.5$ eV and $T = 300$ K are plotted in Fig. 3 as a function of the Matsubara terms counted by n (the corresponding Matsubara frequency is $\xi_n = 2\pi n \frac{k_B T}{\hbar}$) using a moderate damping of $\tau = 10^{-12}$ rad/s. It can be seen that for small frequencies ($n < 7$) the intraband contribution dominates whereas for large frequencies ($n > 7$) the interband contribution dominates the conductivity of graphene and converges to $e^2/4\hbar$ ^{31,34}. By changing the Fermi energy E_F this crossover between the inter- and intraband contribution can be shifted towards lower or larger Matsubara frequencies.

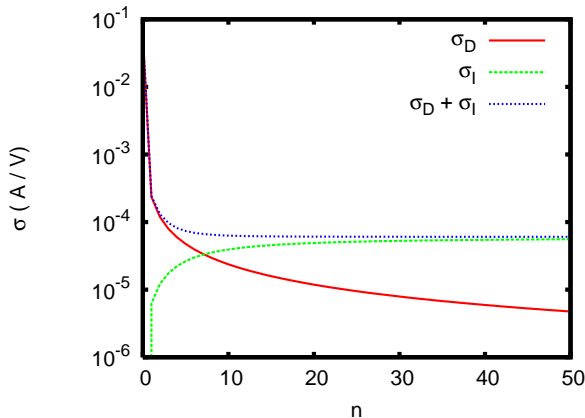


Figure 3. Plot of $\sigma = \sigma_D + \sigma_I$, σ_D , and σ_I as a function of the Matsubara terms.

The reflection coefficients for graphene are different from the expression for a halfspace. On the imaginary axis they are given by⁹

$$r_s = \frac{\tilde{\gamma}_0 - \tilde{\gamma} - \mu_0 \sigma \xi}{\tilde{\gamma}_0 + \tilde{\gamma} + \mu_0 \sigma \xi} \quad \text{and} \quad r_p = \frac{\tilde{\gamma}_0 \epsilon - \tilde{\gamma} + \frac{\sigma \tilde{\gamma} \tilde{\gamma}_0}{\epsilon_0 \xi}}{\tilde{\gamma}_0 \epsilon + \tilde{\gamma} + \frac{\sigma \tilde{\gamma} \tilde{\gamma}_0}{\epsilon_0 \xi}}, \quad (46)$$

where ϵ is in this case the permittivity of the substrate. For a suspended sheet of graphene $\epsilon = 1$ and $\tilde{\gamma} = \tilde{\gamma}_0$.

IV. NUMERICAL RESULTS AND DISCUSSION - ISOTROPIC NANOPARTICLE

A. Gold

In Fig. 4 we first show our results for a spherical gold nanoparticle above a gold halfspace. The resulting values of the CP force are normalized to the case, where the gold halfspace is replaced by an ideal metal, i.e. we use the expression (20) with (27), while the properties of the nanoparticles remain unchanged. Due to this normalization procedure the results are independent of radius of the nanoparticles, but it has to be kept in mind that the presented results are only meaningful for distances d larger than the radius of the nanoparticle. From the numerical results it can be seen that at large distances

the results for the gold halfspace and the ideal metal are the same. For smaller distances the CP force drops with respect to the ideal metal case. Hence, by using a gold halfspace instead of an ideal metal, the force is reduced by about 40% for distances around 100 nm.

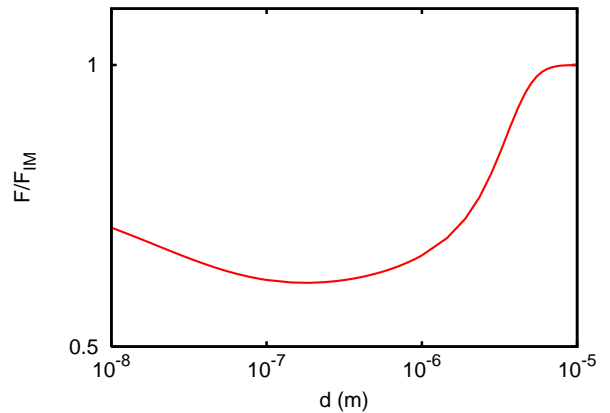


Figure 4. Plots of the CP force of a Au nanoparticle above a Au halfspace as a function of distance d . The force is normalized to the CP force of a gold nanoparticle above an ideal metal. Here and in the following we set $T = 300$ K.

B. Suspended graphene

Now, we replace the gold halfspace by a sheet of suspended graphene. In this case (see Figs. 5) the force coincides with the ideal metal case for large distances $d > \lambda_{th}$. This is due to the fact that for small frequencies (i.e. large distances) the Drude term in the conductivity of graphene dominates. This result has to be taken with some care, since the used model is strictly valid only for frequencies larger than $1/\tau$ ³¹. However, the frequency $1/\tau = 10^{12}$ rad/s corresponds to a distance of about 2 mm which is much larger than the studied distances. Furthermore, this observation is in accordance with results found in Ref.²³ using the Dirac model for graphene¹⁷.

For small distances ($d < \lambda_{th}$) the CP force is relatively small compared to the ideal metal case. The minimal values found are about 7% of the ideal metal case. By increasing the Fermi level the force on the particle can be increased. At $d = 100$ nm one can increase the relative force from about 7% to 12%. Hence, the CP force between a spherical nanoparticle and a sheet of graphene as well as the effect of tuning is rather small. These observations are similar to the results found for the Casimir-Lifshitz force between a gold halfspace and a sheet of graphene^{16,17,19}. In Fig. 5 we also show the results for the force between a gold nanoparticle above a sheet of graphene normalized to the case where graphene is replaced by a gold halfspace. The qualitative behaviour remains the same but the relative values change slightly.

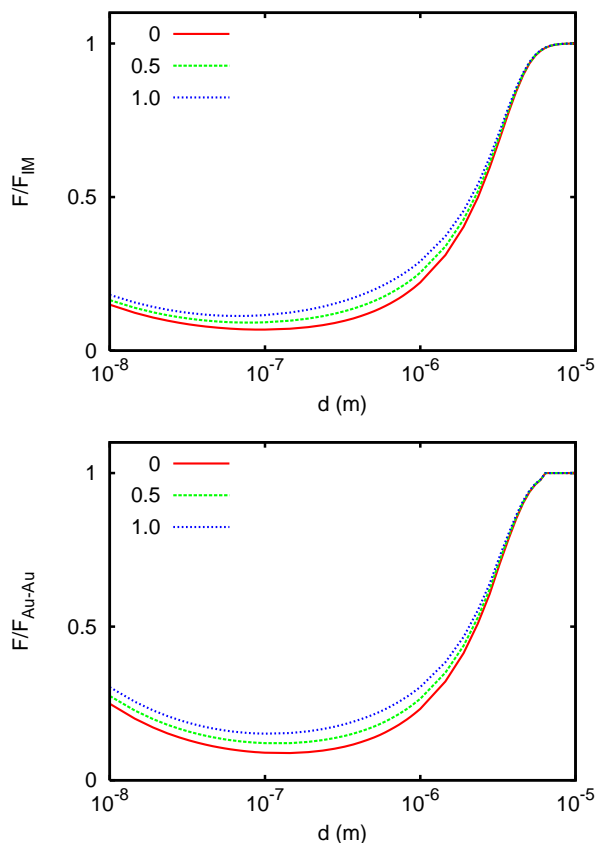


Figure 5. Plots of the CP force of a Au nanoparticle above a suspended sheet of graphene as a function of distance d for different Fermi levels E_F . The results are normalized to the CP force of a Au nanoparticle above an ideal metal (top) or above a gold halfspace (bottom).

V. NUMERICAL RESULTS AND DISCUSSION - SPHEROIDAL NANOPARTICLE

To analyze the influence of the shape of the particle on the CP force we consider now a spheroidal nanoparticle close to a suspended sheet of graphene. To start with, we choose a gold nanoparticle with different aspect ratios R_b/R_a . As can be seen in Fig. 6 the exact CP force variation depends on the distance and the orientation of the nanoparticle as well as the Fermi level of the graphene sheet. For $d = 100$ nm we find that with respect to the spherical particle the force for an oblate nanoparticle ($R_b/R_a > 1$) increases if the rotational axis is oriented parallel to the graphene sheet (x orientation) and first decreases when the nanoparticle becomes slightly prolate ($R_b/R_a < 1$) before it increases rapidly for strongly prolate particles. For the nanoparticle with the rotational axis normal to the graphene sheet the CP force decreases monotonically with the aspect ratio R_b/R_a . Similar trends are found for $d = 1 \mu\text{m}$. Hence, the shape and orientation of the nanoparticle has a strong influence on the force exerted on that parti-

cle. Note that this effect can even be more important than the effect of tuning by changing the Fermi level in graphene.

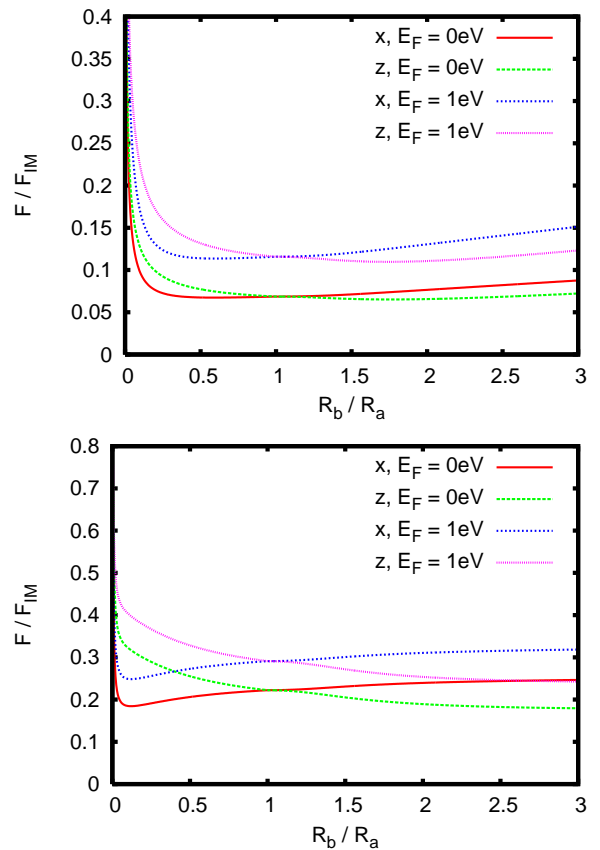


Figure 6. Plots of the CP force of a spheroidal Au nanoparticle above a suspended sheet of graphene as a function of R_b/R_a for different Fermi levels $E_F = 0$ eV, 1 eV and orientations (rotational axis is along x or z axis) choosing $d = 100$ nm (top) and $d = 1 \mu\text{m}$ (bottom). The results are normalized to the CP force of the spheroidal Au nanoparticle above an ideal metal.

In Fig. 7 we show some results of the CP force between a prolate, oblate, and spherical Au nanoparticle and a sheet of graphene (here we use $E_F = 0$ eV) as a function of distance. It can be seen that for distances on the order of 100 nm or smaller the force on the nonspherical particles is generally larger than on the spherical ones having the same volume. For larger distances the force of the spheroidal particles compared to the spherical particles is always larger when the particle axis with larger R_a or R_b is normal to the graphene sheet. On the other hand, if this particle axis with larger R_a or R_b is parallel to the graphene sheet, the resulting force is smaller than for a particle of spherical shape. As observed for spherical particles the CP force converges in all cases to the ideal metal result for $d \gg \lambda_{\text{th}}$. Hence, for such distances graphene acts like a perfect metal regardless of the shape and orientation of the nanoparticle.

In Fig. 8 we show the results for the same configura-

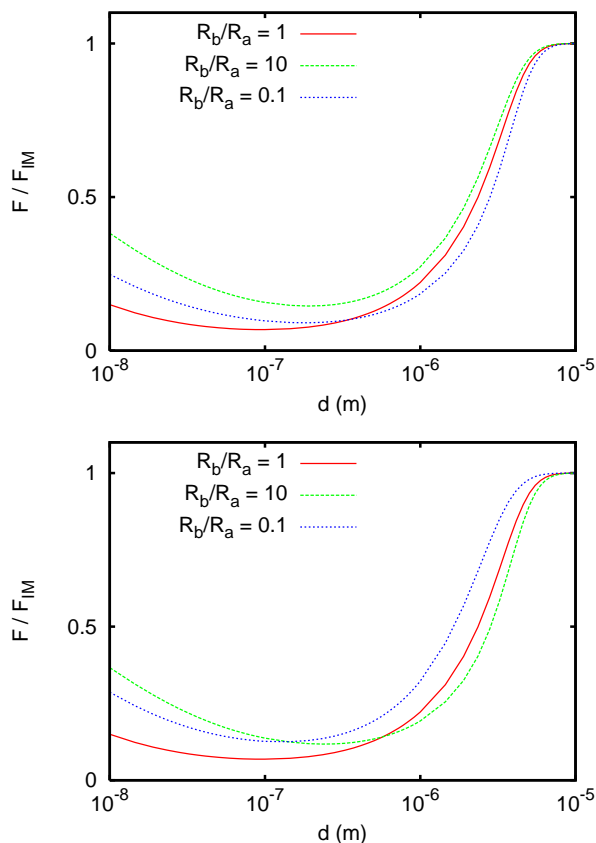


Figure 7. Plots of the CP force of a spheroidal Au nanoparticle above a suspended sheet of graphene as a function of distance choosing a prolate particle with $R_b/R_a = 0.1$, an oblate particle with $R_b/R_a = 10$, and a spherical particle with $R_b/R_a = 1$. The Fermi level of graphene is $E_F = 0$ eV and two different orientations of the nanoparticle are chosen: rotational axis is parallel to the graphene sheet (x orientation, top) or normal to the graphene sheet (z orientation, bottom). The results are normalized to the CP force of the spheroidal Au nanoparticle above an ideal metal.

tion as in Fig. 7 but for graphene with a Fermi level of $E_F = 1$ eV. In this case, the CP force between spheroidal nanoparticles and graphene is much larger than between spherical particles and graphene for distances smaller than 1 micron so that even values between 20-50% of that between a nanoparticle and a perfect metal can be achieved which is huge compared to the values of about 3% or less found in Refs.^{16,17,19} and it is large compared to the value found for the spheroidal nanoparticle which is between 7-15% in Fig. 8 of the ideal metal case.

VI. CONCLUSION

In summary, we have considered the thermal Casimir-Polder interaction between spherical and spheroidal nanoparticles and a sheet of graphene. We have shown that the Casimir-Polder force for spherical particles is

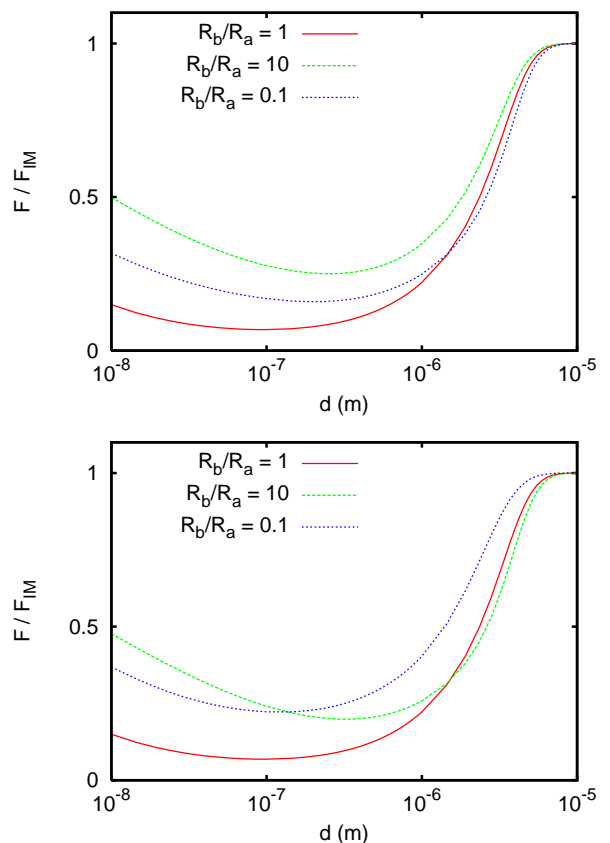


Figure 8. As Fig. 7 but with $E_F = 1$ eV.

in general small compared to the force between the nanoparticle and a perfect metal when considering distances much smaller than the thermal wavelength. On the other hand, for distances larger than the thermal wavelength the sheet of graphene behaves like a perfect metal a result which was also found previously for atoms above graphene. Tuning the electron density inside the sheet of graphene by gating or doping seems to have a relatively small impact on the resulting force. However, when considering spheroidal nanoparticles it turns out that the shape and orientation can have an impact on the resulting force which is larger than that of the tuning inside graphene. Depending on the distance regime the force between spheroidal nanoparticles and graphene can be larger or smaller than that for spherical nanoparticles having the same volume. For distances smaller than 100 nm we find that the force exerted on spheroidal nanoparticles is always larger than for spheroidal nanoparticles with the same volume so that. Since the effect of tuning by means of graphene and the effect of anisotropy and tuning add resulting in a force between spheroidal nanoparticles and graphene which can be in the range of 20-50% of that between spheroidal nanoparticles and a perfect metal. This is quite large compared to the Casimir force found between a gold halfspace and a sheets of graphene or between a

spherical gold nanoparticle and graphene which are about 3% or between 7-15% of that for perfect metals.

-
- ¹ L. Novotny and B. Hecht, Nano-Optics, (Cambridge University Press, Cambridge, 2012).
 - ² I.A. Dorofeyev, J. Phys. D: Appl. Phys. **31**, 600 (1998).
 - ³ J.-P. Mulet, K. Joulain, R. Carminati, J.-J. Greffet, Appl. Phys. Lett. **78**, 2931 (2001).
 - ⁴ M. Tschikin, S.-A. Biehs, P. Ben-Abdallah, F. S. S. Rosa, Eur. Phys. J. B **85**, 233 (2012).
 - ⁵ J. I. Gersten and A. Nitzan, Chem. Phys. Lett. **104**, 31 (1984).
 - ⁶ X. M. Hua, J. I. Gersten, and A. Nitzan, J. Chem. Phys. **83**, 3650 (1985).
 - ⁷ G. S. Agarwal and S.-A. Biehs, Opt. Lett. **38**, 4421 (2013).
 - ⁸ P. W. Milonni, The Quantum Vacuum, (Academic Press, 1994).
 - ⁹ F. H. L. Koppens, D. E. Chang, and F. J. Garcia de Abajo, Nano Lett. **11**, 3370 (2011).
 - ¹⁰ R. Messina, J.-P. Hugonin, J.-J. Greffet, F. Marquier, Y. De Wilde, A. Belarouci, L. Frechette, Y. Cordier, and P. Ben-Abdallah, Phys. Rev. B **87**, 085421 (2013).
 - ¹¹ V. B. Svetovoy, P. J. van Zwol, J. Chevrier, Phys. Rev. B **85**, 155418 (2012); O. Ilic, M. Jablan, J. D. Joannopoulos, I. Celanovic, H. Buljan, and M. Soljačić, Phys. Rev. B **85**, 155422 (2012).
 - ¹² S.-A. Biehs and G. S. Agarwal, Appl. Phys. Lett. **103**, 243112 (2013).
 - ¹³ A. H. Castro Neto, F. Guinea, N. M. R. Peres, K. S. Novoselov, and A. K. Geim, Rev. Mod. Phys. **81**, 109 (2009).
 - ¹⁴ G. Gómez-Santoz, Phys. Rev. B **80**, 245424 (2009).
 - ¹⁵ D. Drosdoff and L. Woods, Phys. Rev. B **82**, 155459 (2010).
 - ¹⁶ B. E. Sernelius, Eur. Phys. Lett. **95**, 57003 (2011).
 - ¹⁷ M. Bordag, I. V. Fialkovsky, D. M. Gitman, and D. V. Vassilevich, Phys. Rev. B **80**, 245406 (2009).
 - ¹⁸ I. V. Fialkovsky, V. N. Marachevsky, and D. V. Vassilevich, Phys. Rev. B **85**, 035446 (2011).
 - ¹⁹ B. E. Sernelius, Phys. Rev. B **85**, 195427 (2012).
 - ²⁰ V. Svetovoy, Z. Moktadir, M. Elwenspoek, and H. Mizuta, Eur. Phys. Lett. **96**, 14006 (2011).
 - ²¹ W.-K. Tse and A. H. MacDonald, Phys. Rev. Lett. **109**, 236806 (2012).
 - ²² V. B. Bezerra, G. L. Klimchitskaya, V. M. Mostepanenko, and C. Romero, Phys. Rev. D **81**, 055003 (2010).
 - ²³ G. L. Klimchitskaya and V. M. Mostepanenko, Phys. Rev. A **89**, 012516 (2014).
 - ²⁴ S. Ribeiro and S. Scheel, Phys. Rev. A **88**, 042519 (2013).
 - ²⁵ P.M. Tomchuk, N.I. Grigorchuk, Phys. Rev. B **73**, 155423 (2006).
 - ²⁶ P.-O. Chapuis, M. Laroche, S. Volz, J.-J. Greffet, Phys. Rev. B **77**, 125402 (2008).
 - ²⁷ O. Huth, F. Rüting, S.-A. Biehs, and M. Holthaus, Eur. Phys. J. Appl. Phys. **50**, 10603 (2010).
 - ²⁸ J. F. Babb, G. L. Klimchitskaya, and V. M. Mostepanenko, Phys. Rev. A **70**, 042901 (2004).
 - ²⁹ L.D. Landau and E.M. Lifshitz, Electrodynamics of Continuous Media (Pergamon, Oxford, 1960).
 - ³⁰ N.W. Ashcroft, N.D. Mermin, Solid State Physics (Harcourt, Fort Worth, 1976).
 - ³¹ L. A. Falkovsky and A. A. Varlamov, Eur. Phys. J. B **56**, 281 (2007).
 - ³² L. A. Falkovsky, J. Phys.: Conf. Ser. **129**, 012004 (2008).
 - ³³ T. Stauber, arXiv:1310.4296v1.
 - ³⁴ T. Stauber, N. M. R. Peres, and A. K. Geim, Phys. Rev. B **78**, 085432 (2008).